Crystal field effects on spin pumping

Cahaya, Adam B.; Leon, Alejandro O.; Bauer, Gerrit E.W.

DOI
10.1103/PhysRevB.96.144434

Publication date
2017

Document Version
Final published version

Published in
Physical Review B

Crystal field effects on spin pumping

Adam B. Cahaya,[1] Alejandro O. Leon,[1] and Gerrit E. W. Bauer[1,2,3]
[1]*Institute for Materials Research, Tohoku University, Sendai 980-8577, Japan*
[2]*WPI-AIMR & CSRN, Tohoku University, Sendai 980-8577, Japan*
[3]*Zernike Institute for Advanced Materials, Groningen University, The Netherlands*
(Received 7 September 2017; published 26 October 2017)

"Spin pumping" is the injection of spin angular momentum by a time-dependent magnetization into an adjacent normal metal proportional to the spin mixing conductance. We study the role of electrostatic interactions in the form of crystal fields on the pumped spin currents generated by insulators with exchange-coupled local moments at the interface to a metal. The crystal field is shown to render the spin currents anisotropic, which implies that the spin mixing conductance of insulator | normal metal bilayers depends on crystal cut and orientation. We interpret the interface "effective field" (imaginary part of the spin mixing conductance) in terms of the coherent motion of the equilibrium spin density induced by proximity in the normal metal.

DOI: 10.1103/PhysRevB.96.144434

I. INTRODUCTION

The interaction between the magnetization and currents in small structures and devices has attracted much attention in the last two decades. The generation of a spin current by magnetization dynamics is referred to as spin pumping [1,2]: A time-dependent magnetization "pumps" a spin current with magnitude and polarization $\mathbf{J} = g_r^{\uparrow\downarrow}\mathbf{m}\times\dot{\mathbf{m}} - g_i^{\uparrow\downarrow}\dot{\mathbf{m}}$ into a normal metal contact, where $\mathbf{m}$ is the unit magnetization vector, $\dot{\mathbf{m}}$ its time derivative, and $g^{\uparrow\downarrow} = g_r^{\uparrow\downarrow} + ig_i^{\uparrow\downarrow}$ is the complex interfacial spin mixing conductance. The spin pumping enhances the magnetization damping and can be interpreted as the Onsager reciprocal effect to the current-induced spin transfer torque, both being governed by the same spin mixing conductance [3]. The mixing conductance of the magnetic insulator yttrium iron garnet (YIG) was predicted to be of the same order of magnitude as that of magnetic metals [4], which was subsequently confirmed by experiments [5,6]. A dependence of the spin mixing conductance on the interface cut and orientation to the normal metal has also been predicted [4] and confirmed [7,8]. This anisotropy could partly be explained by the density of the local Fe magnetic moment directly at the interface. The rotational symmetry of magnetic atoms can be broken by the electric fields generated by neighboring atoms, i.e., the so called *crystal field*. The relationship between the spin pumping and the local symmetry of magnetic moments at the interface has, to the best of our knowledge, not been studied yet. We therefore focus here on noncubic crystal fields of $3d$ transition metal ions with partially (not fully or half-) filled shells. These are predicted to cause effects that are much stronger than those generated by a cubic crystal field or when acting on $4f$ moments. Also, in the former case the spin orbit interaction is much weaker than the spin orbit interaction that we, hence, disregard here.

Under crystal fields, the angular part of the single $3d$ electron is described by the real valued doubly degenerate e_g and triply degenerate t_{2g} orbitals [9,10]. For transition metal ions on sites with octahedral symmetry, the energy level order is $E_{e_g} > E_{t_{2g}}$ while in tetrahedral environment $E_{t_{2g}} > E_{e_g}$ [9,10]. The total orbital angular momentum in this basis is quenched, $\langle L_z\rangle = 0$ [9,10]. The magnetism is then predominantly caused by the electron (Pauli) spins. When the spin orbit interaction is not negligible but competes with the crystal fields, the eigenstates are complex combinations of the sets e_g and t_{2g}. The orbital moment is then not completely quenched $\langle L_z\rangle \neq 0$ and the energy depends on the direction of the magnetization relative to the crystal axes (magnetic anisotropy) [11]. The effects of the spin-orbit interaction is discussed in a forthcoming paper with emphasis on partially filled $4f$ shells [12].

Here we study the role of crystal fields on the spin mixing conductance that governs spin pumping and other properties of interfaces. The paper is organized as follows. In Sec. II, we review the static and dynamics of $3d$ transition metal magnetic moments, disregarding their weak spin-orbit interactions. In the presence of crystal fields, the ground state electronic density of individual ions is nonspherical. By the exchange interaction such local moment induces in a metal an oscillating proximity spin density and associated Ruderman-Kittel-Kasuya-Yosida interaction (RKKY) [13–15] that are also anisotropic. This has, for example, been confirmed by first principles calculations on metallic surfaces [16]. The effects of such anisotropies on the spin dynamics are discussed in Sec. III, where we find that the spin current emitted by a dynamic magnetization is enhanced in certain directions. We discuss how the anisotropy influences local magnetization dynamic in term of enhanced damping in Sec. IV. In Sec. V, we extend our analysis to magnetic insulators in which the local moments at the interface are exposed to normal metal contacts. In Sec. VI we conclude that the crystal fields induce differences in the spin pumping for different crystal growth directions, which might help to explain some experiments.

II. SINGLE-ION MODEL

Consider a single localized magnetic moment generated by a partially filled $3d$ shell with spin density $\mathbf{S}_d(\mathbf{r},t)$ that depends adiabatically on time. In terms of the single electron wave functions $\psi_j(\mathbf{r})$ with orbital index j, the ground state spin density reads

$$\mathbf{S}_d(\mathbf{r},t) = \mathbf{S}(t)n_d(\mathbf{r}), \tag{1}$$

where the electron density distribution of unpaired electrons

$$n_d(\mathbf{r}) = \sum_j S_j|\psi_j(\mathbf{r})|^2, \tag{2}$$

$$S_j = \frac{f_{j,\uparrow} - f_{j,\downarrow}}{\sum_k (f_{k,\uparrow} - f_{k,\downarrow})} \tag{3}$$

TABLE I. The deformation of the spin density of $3d$ orbitals can be expressed in terms of the quadrupole moment Q_2, which is obtained from this table and the occupation numbers.

Orbital Y_j	$\langle\Omega\rangle_j$
Y_{z^2}	4/7
$Y_{x^2-y^2}$ and Y_{xy}	−4/7
Y_{xz} and Y_{yz}	2/7

depends on the occupation numbers f_{j,m_s} of orbital j and spin label $m_s = \{\uparrow,\downarrow\}$ and is normalized, $\int d\mathbf{r}\, n_d(\mathbf{r}) = 1$. The occupation numbers f_{j,m_s} are governed by the *aufbau* principle when the thermal energy is much smaller than the crystal field splitting (Δ), i.e., $k_B T/|\Delta| \ll 1$, where k_B is the Boltzmann constant and T the temperature. Since spin orbit interaction is disregarded, the time dependence is encoded exclusively in the unit vector of the total spin $\mathbf{S}(t)$.

In the presence of crystal fields, $n_d(\mathbf{r})$ has the point symmetry of the crystal site (or higher) that is characterized by a multipolar expansion. Here we focus on the common case of uniaxial deformation along the z direction, which allows parameterizing of the anisotropy in the spin density by its quadrupole moment

$$Q_2 = \int d\mathbf{r} r^2 \left(\frac{3z^2}{r^2} - 1\right) n_d(\mathbf{r}), \tag{4}$$

where $z = r\cos\theta$ is the coordinate along the symmetry axis of $n_d(\mathbf{r})$. $Q_2 > 0 (< 0)$ describes a prolate (oblate) ellipsoidlike distribution. Decomposing the orbitals in the radial and angular functions, $\psi_j(\mathbf{r}) = R_{3d}(r) Y_j(\mathbf{\Omega})$, the quadrupole reads

$$Q_2 = \langle r^2\rangle \sum_j S_j \int (3\cos^2\theta - 1)|Y_j(\Omega)|^2 d\mathbf{\Omega}, \tag{5}$$

where $r = |\mathbf{r}|$, $\langle r^2\rangle = \int r^2 dr r^2 R_{3d}^2(r)$, $\Omega \equiv \mathbf{r}/r$ and $d\mathbf{\Omega} = d\theta d\phi \sin\theta$. The radial function $R_{3d}(r)$ can be approximated by Slater-type orbitals [17,18], while the angular function are linear combinations of spherical harmonics (see Appendix A). Q_2 is calculated using the occupation numbers and the coefficients $\langle\Omega\rangle_j = \int (3\cos^2\theta - 1)|Y_j(\mathbf{\Omega})|^2 d\mathbf{\Omega}$, listed in Table I.

Crystal fields can be parameterized by a *point charge model* of the local environment. The Hamiltonian close to the center of an octahedron made from point charges qe is

$$H_{cf}(\mathbf{r}) = \sum_n \frac{-qe^2}{4\pi\varepsilon_0|\mathbf{r} - \mathbf{r}_n|} \simeq \frac{-3qe^2}{2\pi\varepsilon_0 R_0} + \Delta_{\text{octa}} \frac{x^4 + y^4 + z^4 - 3(x^2y^2 + x^2z^2 + y^2z^2)}{\langle r^4\rangle}, \tag{6}$$

where the subscript n labels the point charges at $\{(\pm R_0,0,0),(0,\pm R_0,0),(0,0,\pm R_0)\}$, $\mathbf{r} = x\hat{\mathbf{x}} + y\hat{\mathbf{y}} + z\hat{\mathbf{z}}$, and the Cartesian axes $\{x,y,z\}$ are oriented along the crystallographic directions (100), (010), and (001), respectively. R_0 is the nearest-neighbor distance, ε_0 is the vacuum permittivity, $-e$ is the electron charge, and qe is the electric charge of neighboring ions. In metals, ion cores are positively charged, i.e., $q > 0$, while in transition metal oxides the oxygen anions dominate and $q < 0$. The crystal field parameter is $\Delta_{\text{octa}} = -7qe^2\langle r^4\rangle R_0^{-5}(8\pi\varepsilon_0)^{-1}$ and can be estimated as $\Delta \sim 2$ eV for $q = -2$, $\langle r^4\rangle^{1/4} = 1.5$ Å, $R_0 = 3$ Å. In the tetrahedral site, on the other hand, the magnetic atom sits in the center of a cube defined by $(\pm R_0, \pm R_0, \pm R_0)/\sqrt{3}$. Both octahedral and tetrahedral sites are described by the same Hamiltonian [10] but $\Delta_{\text{tetra}} = -4\Delta_{\text{octa}}/9$. Figure 1(b) shows the crystal field splitting for a symmetric octahedron (charges equidistant from the origin) into a doubly degenerate e_g and triply degenerate t_{2g} states (see Appendix). Uniaxial strain breaks the degeneracies of e_g and t_{2g} levels [19–21] as sketched in Figs. 1(a) and 1(c).

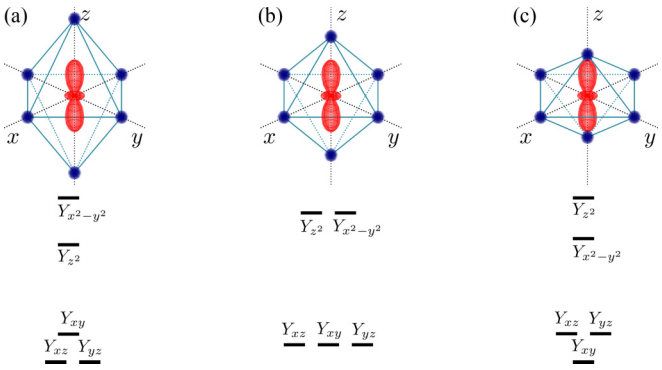

FIG. 1. The Y_{z^2} orbital of a $3d$ magnetic ion in an octahedral environment (upper panel) and the corresponding orbital splitting of the real-valued orbitals $e_g(Y_{z^2}, Y_{x^2-y^2})$ and $t_{2g}(Y_{xy}, Y_{xz}, Y_{yz})$ (lower panel). The octahedral environment is (a) elongated, (b) unperturbed, and (c) compressed in the z direction.

Half-filled shells, such as Mn^{2+} and $Fe^{3+}$are isotropic (spherical) and their Q_2 vanishes in any crystal field. The quadrupolar moments vanish as well for octahedral and tetrahedral crystal fields, because the half-filled e_g and t_{2g} shells are still nearly spherical:

$$e_g : \int d\mathbf{\Omega}(3\cos^2\theta - 1)(|Y_{z^2}|^2 + |Y_{x^2-y^2}|^2) = 0, \tag{7}$$

$$t_{2g} : \int d\mathbf{\Omega}(3\cos^2\theta - 1)(|Y_{xy}|^2 + |Y_{xz}|^2 + |Y_{yz}|^2) = 0. \tag{8}$$

The quadrupole in the presence of compressive and tensile uniaxial strains depends on the occupation numbers as

$$\frac{Q_2}{\langle r^2\rangle} = \frac{2}{7}\left[S_{Y_{xz}} + S_{Y_{yz}} + 2\left(S_{Y_{z^2}} - S_{Y_{x^2-y^2}} - S_{Y_{xy}}\right)\right], \tag{9}$$

where S_{Y_j} is given by Eq. (3). We note that even in distorted octahedral sites, some ions such as V^{2+}, Cr^{3+} Ni^{2+}, and Cu^{3+} have $Q_2 = 0$ because the e_g and t_{2g} are half filled.

Interaction between a magnetic ion and conduction electrons

The interaction between localized magnetic moments and conduction electrons with spin density $\mathbf{s}_c(\mathbf{r},t)$ is described by the s-d exchange Hamiltonian [22,23]. In the local-density approximation:

$$H_{\text{s-d}} = -\frac{J}{\hbar^2}\int \mathbf{S}_d(\mathbf{r},t)\cdot\mathbf{s}_c(\mathbf{r},t) d\mathbf{r}, \tag{10}$$

where in the static and strong screening limit of the Coulomb interaction the exchange constant $J = g_e^{-1}$ is the reciprocal conduction electron density of states g_e of the host metal

and $\hbar$ is Planck's constant divided by 2π. For free electrons, $g_e = m_e k_F/(\pi^2\hbar^2) = 3n_e/(2E_F)$, in terms of the electron density n_e, Fermi energy E_F, and the effective electron mass m_e. In the ground state, a static magnetic moment induces spin density oscillations. $H_{\rm s-d}$ also communicates the time dependence of the magnetic moment $\dot{\mathbf{S}} \neq 0$ to the conduction electrons, which can be formulated by extending the RKKY perturbation theory into the time domain [2]. Magnetization dynamics can be excited by magnetic or spin resonance, but also by spin transfer torques due to voltage and temperature gradients, lattice vibrations, etc. [24,25].

For sufficiently weak coupling, the response of the conduction electrons to a time dependent local moment $\mathbf{S}_d(\mathbf{r},t)$ reads

$$\mathbf{s}_c(\mathbf{r},t) = \frac{J}{\hbar^2}\int d\mathbf{r}'dt'\chi(\mathbf{r}-\mathbf{r}',t-t')\mathbf{S}_d(\mathbf{r}',t'), \tag{11}$$

where $\chi(\mathbf{r},t)$ is the (scalar) dynamic spin susceptibility of the homogeneous host metal. In frequency and momentum space

$$\mathbf{s}_c(\mathbf{q},\omega) = \frac{J}{\hbar^2}\chi(q,\omega)\mathbf{S}_d(\mathbf{q},\omega), \tag{12}$$

where

$$f(\mathbf{q},\omega) = \int d\mathbf{r}\int dt f(\mathbf{r},t)e^{-i\mathbf{q}\cdot\mathbf{r}}e^{i\omega t}, \tag{13}$$

$$f(\mathbf{r},t) = \int \frac{d\mathbf{q}}{(2\pi)^3}\int \frac{d\omega}{2\pi} f(\mathbf{q},\omega)e^{i\mathbf{q}\cdot\mathbf{r}}e^{-i\omega t}. \tag{14}$$

Here the integration domain is a large system volume. In the free electron gas

$$\chi(q,\omega) = \sum_{\mathbf{p}}\frac{(f_{\mathbf{p}}-f_{\mathbf{p}+\mathbf{q}})\hbar^2/2}{\epsilon_{\mathbf{p}+\mathbf{q}}-\epsilon_{\mathbf{p}}+\hbar\omega+i0^+}, \tag{15}$$

where $f_{\mathbf{p}} = [\exp[(\epsilon_{\mathbf{p}}-\mu)/(k_BT)]+1]^{-1}$ is the Fermi-Dirac distribution, $\epsilon_{\mathbf{p}} = \hbar^2p^2/(2m_e)$, μ is chemical potential, and 0^+ is a positive infinitesimal. The time constants of the conduction electrons in high density metals are governed by the Fermi velocity (fs) and are much smaller than that of the magnetization dynamics (ns), which justifies expansion to leading order in the characteristic frequencies, i.e., the adiabatic approximation [2], $\chi(q,\omega)\simeq\chi_r(q)+i\omega\chi_i(q)$, where $\chi_r(q) = \lim_{\omega\to0}\mathrm{Re}\,\chi(q,\omega)$ and $\chi_i(q) = \lim_{\omega\to0}\partial_\omega\,\mathrm{Im}\,\chi(q,\omega)$. In the three-dimensional free electron gas, the real part of the static susceptibility $\chi_r(r)$ and its Fourier transform $\chi_r(q)$ correspond to the static RKKY and Lindhard functions

$$\chi_r(r) = \frac{g_e\hbar^2}{16\pi r^3}\left(\frac{\sin 2k_Fr}{2k_Fr}-\cos 2k_Fr\right), \tag{16}$$

$$\chi_r(q) = \frac{g_e\hbar^2}{8}\left(1+\frac{k_F^2-(q/2)^2}{k_Fq}\ln\left|\frac{k_F+q/2}{k_F-q/2}\right|\right), \tag{17}$$

respectively [26]. The imaginary part of the susceptibility is

$$\chi_i(r) = \frac{g_e^2\hbar^3\pi}{8}\frac{\sin^2 k_Fr}{k_F^2r^2}, \tag{18}$$

$$\chi_i(q) = \frac{g_e^2\hbar^3\pi^3}{8k_F^2q}\Theta(2k_F-q), \tag{19}$$

where $k_F = (3\pi^2n_e)^{1/3}$ is the Fermi wave number. Using Eq. (1)

$$\mathbf{s}_c(\mathbf{q},\omega) = \frac{J}{\hbar^2}\mathbf{S}(\omega)\chi(q,\omega)[n_{\rm iso}(q)+n_{\rm ani}(\mathbf{q})]. \tag{20}$$

The Fourier transform of the density distribution $n_d = n_{\rm iso}(r)+n_{\rm ani}(\mathbf{r})$ is the sum of

$$n_{\rm iso}(q) = \langle j_0(qr)\rangle \tag{21}$$

and

$$n_{\rm ani}(\mathbf{q}) = -\pi\langle j_2(qr)\rangle Y_{z^2}\left(\frac{\mathbf{q}}{q}\right)\sqrt{\frac{5}{\pi}}\frac{Q_2}{\langle r^2\rangle} \tag{22}$$

$$= -\frac{5Q_2}{4\langle r^2\rangle}\langle j_2(qr)\rangle(3\cos^2\theta_{\mathbf{q}}-1), \tag{23}$$

with $\cos\theta_{\mathbf{q}} = \mathbf{q}\cdot\hat{\mathbf{z}}$ and $\langle j_n(qr)\rangle$ is the expectation value of the nth spherical Bessel function for a radial $3d$ wave function. Explicit formulas for $\langle j_0(qr)\rangle$ and $\langle j_2(qr)\rangle$ are demoted to the Appendix A 1.

Substituting $\chi(q,\omega)\simeq\chi_r(q)+i\omega\chi_i(q)$ and keeping only linear terms in the frequency ω (adiabatic approximation)

$$\mathbf{s}_c(\mathbf{q},\omega) = \frac{J}{\hbar^2}[\mathbf{S}(\omega)\chi_r(q)+i\omega\mathbf{S}(\omega)\chi_i(q)]n_d(\mathbf{q}). \tag{24}$$

Transforming back into time domain

$$\mathbf{s}_c(\mathbf{r},t) = \frac{J}{\hbar^2}[\rho_r(\mathbf{r})\mathbf{S}(t)-\rho_i(\mathbf{r})\dot{\mathbf{S}}(t)]. \tag{25}$$

The densities

$$\rho_r(\mathbf{r}) = \int\frac{d\mathbf{q}e^{i\mathbf{q}\cdot\mathbf{r}}}{(2\pi)^3}\chi_r(q)n_d(\mathbf{q}) \tag{26}$$

$$\rho_i(\mathbf{r}) = \int\frac{d\mathbf{q}e^{i\mathbf{q}\cdot\mathbf{r}}}{(2\pi)^3}\chi_i(q)n_d(\mathbf{q}) \tag{27}$$

are plotted in Fig. 2 for several values of $k_F^2\langle r^2\rangle$ and Q_2. Figures 2(a) and 2(c) illustrate that with increasing Fermi energy a larger region of the electron gas is polarized, as in the RKKY polarization function (16). The ion anisotropy is parameterized by the quadrupole Q_2, which is proportional to $\langle r^2\rangle$, see Eq. (5); larger ions induce a stronger anisotropy, cf. Figs. 2(c) and 2(d). This can also be seen from Eq. (23) by approximating $\langle j_2(qr)\rangle\approx q^2\langle r^2\rangle/15$, which leads to $n_{\rm ani}\sim\langle r^2\rangle$. The sign of Q_2 can enlarge or decrease the total conduction electron spin polarization, as shown in Figs. 2(c) and 2(e).

When the atomic radius is small $n_d(\mathbf{r})\to\delta(\mathbf{r})$, the static spin polarization reduces to the well-known RKKY spatial oscillations

$$\lim_{n_d(\mathbf{r})\to\delta(\mathbf{r})}\rho_r(\mathbf{r}) = \chi_r(r),$$

while $\rho_i(\mathbf{r})\to\chi_i(r)$. In this limit all crystal field effects vanish.

III. SPIN CURRENT

Conduction electron spin density and local moments are also related by the spin conservation equation

$$\partial_t\mathbf{s}_c(\mathbf{r},t)+\nabla\cdot\mathbb{J}(\mathbf{r}) = \left(\frac{d\mathbf{s}_c(\mathbf{r},t)}{dt}\right)_{\rm source}, \tag{28}$$

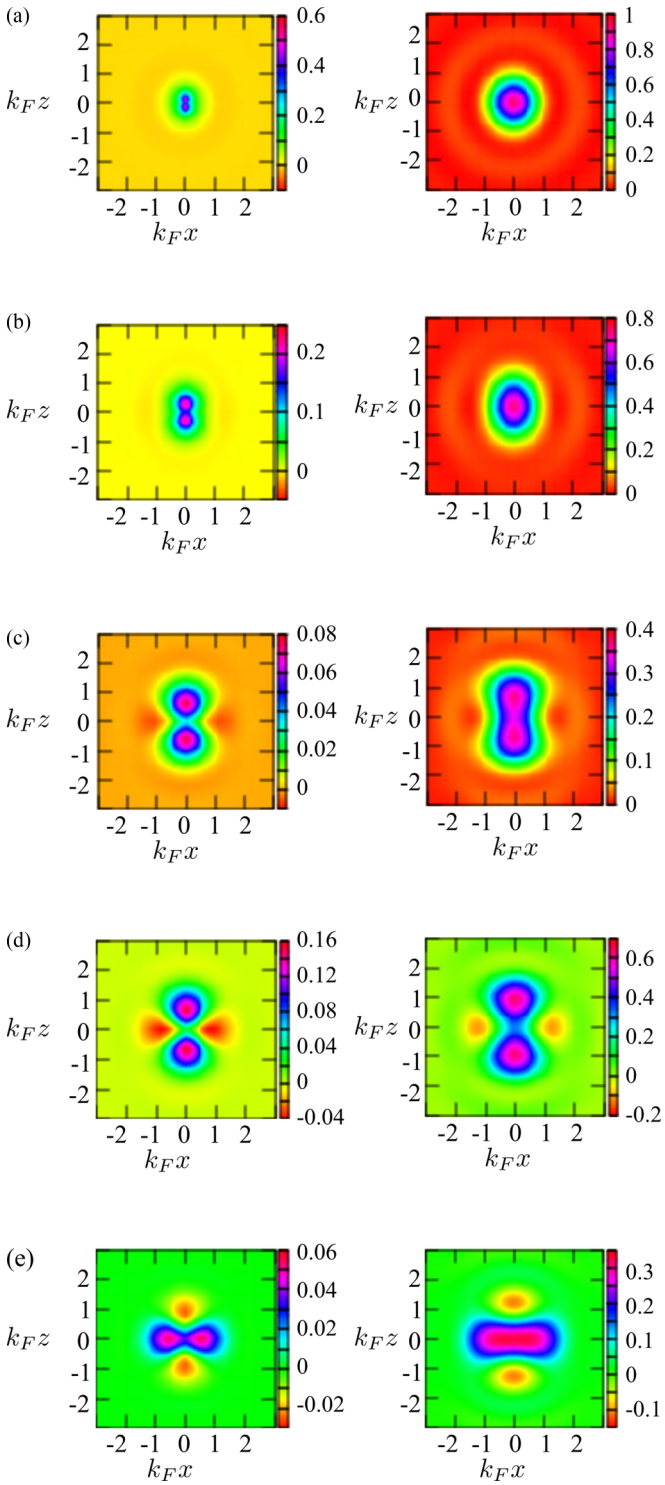

FIG. 2. Conduction electron spin densities induced by a time-dependent anisotropic magnetic moment. $\rho_r(\mathbf{r})$ (left panels) and $\rho_i(\mathbf{r})$ (right panels) as defined in Eq. (25) are plotted for several parameter values in the $y = 0$ plane. $\rho_r(\mathbf{r})$ and $\rho_i(\mathbf{r})$ are normalized to $2k_F^2 g_e$ and $\chi_i(r = 0)$, respectively. The values of $(k_F^2\langle r^2\rangle, Q_2/\langle r^2\rangle)$ are (a) (1/4,1/7), (b) (1,1/7), (c) (4,1/7), (d) (4,8/21), (e) (4, − 1/7).

where the source term

$$\left(\frac{d\mathbf{s}_c(\mathbf{r},t)}{dt}\right)_{\text{source}} = -\frac{\mathbf{s}_c(\mathbf{r},t)}{\tau_s} + \frac{J}{\hbar^2}\mathbf{s}_c(\mathbf{r},t)\times\mathbf{S}_d(\mathbf{r},t), \tag{29}$$

describes spin flip scattering on the time scale τ_s and spin precession in the exchange torque exerted by the local moment. $\mathbb{J}_\sigma^\nu$ is the spin current tensor, where the indexes σ and ν refer to the spin polarization and current directions, respectively [27]. We obtain explicit expressions for the spin current divergence by substituting $\mathbf{s}_c$ from Eq. (25), in the clean limit of the metal and slow magnetization dynamics ($\tau_s \to \infty$ and $\ddot{\mathbf{S}} \to 0$):

$$\nabla\cdot\mathbb{J}(\mathbf{r}) = \frac{J^2}{\hbar^4}\rho_i(\mathbf{r})n_{3d}(\mathbf{r})\mathbf{S}\times\dot{\mathbf{S}} - \frac{J}{\hbar^2}\rho_r(\mathbf{r})\dot{\mathbf{S}}. \tag{30}$$

By writing the spin current in terms of a vector spin potential $\mathbf{\Phi}(\mathbf{r})$ as $\mathbb{J}_\sigma^\nu(\mathbf{r}) = -\partial_\nu\mathbf{\Phi}(\mathbf{r})$, Eq. (30) is reduced to a Poisson equation. The spin current direction is governed by the gradient of the spin potential, while its polarization is proportional to its direction. The solution of our Poisson equation is

$$\mathbf{\Phi}(\mathbf{r},t) = \Phi_r(\mathbf{r})\mathbf{S}(t)\times\dot{\mathbf{S}}(t) + \Phi_i(\mathbf{r})\dot{\mathbf{S}}(t), \tag{31}$$

where we defined dissipative (Φ_r) and reactive (Φ_i) scalar potentials. To leading order in the quadrupole moment

$$\Phi_r(\mathbf{r}) = \frac{G_r^{\text{iso}}}{4\pi r}\left(1 + \frac{3\cos^2\theta - 1}{4r^2}Q_2\right), \tag{32}$$

where

$$G_r^{\text{iso}} \equiv \frac{J^2}{\hbar^4}\int\frac{d\mathbf{q}}{(2\pi)^3}\chi_i(q)|n_d(\mathbf{q})|^2, \tag{33}$$

$$= G_r\left[F_0 + \left(\frac{Q_2}{\langle r^2\rangle}\right)^2 F_2\right], \tag{34}$$

with

$$G_r = \frac{\pi J^2 g_e^2}{8\hbar}. \tag{35}$$

The dimensionless parameters can be obtained analytically as:

$$F_0 = \frac{11D(1208 - 5D(27D(3D - 16) + 682)) - 1627}{31185D(D+1)^{11}} + \frac{1627}{31185D}, \tag{36}$$

$$F_2 = \frac{-44D(D(27D(12D - 43) + 985) + 197) - 788}{31185D(D+1)^{11}} + \frac{788}{31185D}, \tag{37}$$

where $D = k_F^2\langle r^2\rangle/14$, and are given in Fig. 3 for various transition metal atoms. With increasing ionic radius, F_0 decreases, but F_2 increases up to half of F_0 for lighter ions, because the ratio of the anisotropic contribution $\langle j_2(qr)\rangle^2/\langle j_0(qr)\rangle^2$ is suppressed for small $\langle r^2\rangle$ [see Eq. (A11)].

When $k_F^2\langle r^2\rangle \to \infty$, both F_0 and F_2 converge to zero as $\sim(k_F^2\langle r^2\rangle)^{-1}$. While for small $k_F^2\langle r^2\rangle \ll 1$, $F_0 \approx 1$, $F_2 \approx 4(k_F^2\langle r^2\rangle)^2/135$ and G_r^{iso} reduces to G_r. $\Phi_r(\mathbf{r})$ decays monotonically with r, but with an anisotropic component. The "reactive" spin potential in the "far field" $r^2 \gg \langle r^2\rangle$ reads to leading order in r^{-1}

$$\Phi_i(\mathbf{r}) = \left(\frac{1}{k_F^2} + Q_2\frac{3\cos^2\theta - 1}{3}\right)\frac{G_i\cos 2k_F r}{16\pi r^3}, \tag{38}$$

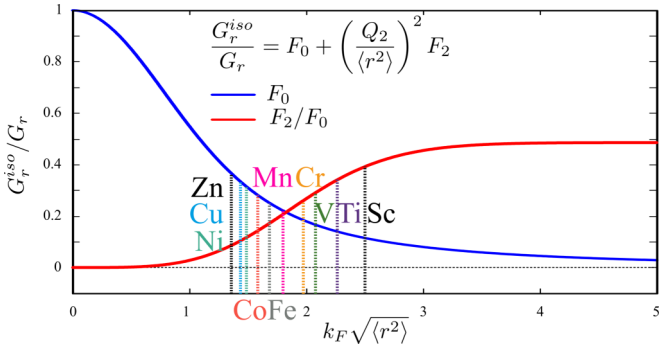

FIG. 3. Real (dissipative) part of the spin mixing conductance $G_r^{\rm iso}/G_r$ as defined in Eqs. (34) and (35) for $3d$ local moments in a free electron metal with Fermi number $k_F \sim 2\,\text{Å}^{-1}$ as a function of $\langle r^2\rangle$, the mean square $3d$ orbital radius. The suppression of F_0 with increasing $\langle r^2\rangle$ reflects the reduced Fourier components of exchange scattering at the Fermi surface. Also indicated are the average $3d$ radii of free transition metal atoms [18] that decrease with higher nuclear charge.

where $G_i = Jg_e/4$. It oscillates as a function of distance as $\cos(2k_F r)$, in phase with the RKKY-like ground state spin density.

We can decompose the spin current along the radial $\hat{\mathbf{r}}$ and polar $\hat{\boldsymbol{\theta}}$ unit vectors as

$$\mathbf{J}^r(\mathbf{r}) = \frac{1}{4\pi r^2}\left(G_i f_2(\theta)\frac{\sin 2k_F r}{2k_F r} + f_1(\theta)G_r\mathbf{S}\times\right)\dot{\mathbf{S}}, \quad (39)$$

$$\mathbf{J}^\theta(\mathbf{r}) = \frac{3Q_2\cos\theta\sin\theta}{8\pi r^4}\left[\frac{G_i\cos 2k_F r}{3k_F r} - G_r\mathbf{S}\times\right]\dot{\mathbf{S}}, \quad (40)$$

respectively, where $f_1(\theta) = 1 + 3Q_2(3\cos^2\theta - 1)/(4r^2)$, $f_2(\theta) = 1 + (2/3)k_F^2 Q_2(3\cos^2\theta - 1)$. The azimuthal $\mathbf{J}^\varphi$ vanishes by symmetry. Ions with half-filled shells are spherically symmetric and pump a radially symmetric spin current, i.e., $\mathbf{J}^\theta \equiv 0$.

The theory as exposed above is directly applicable to magnetic impurities in a metal host. It induces anisotropy into the RKKY interaction between magnetic moments in dilute alloys, which can be relevant for the Kondo and related effects. Here we do not pursue this direction, since we are mainly interested in the dynamics of interfaces between magnetic insulators and metals.

In transition metal oxides, magnetic cations usually fill the voids created by oxygen anions scaffolding, with commonly tetrahedral and octahedral coordination. In order to generate finite Q_2, the symmetry must be broken by, e.g., by strain or at interface. This effect is at least partly responsible for the large interface (compared to bulk) magnetic anisotropy of transition metals [28].

IV. LOCAL MAGNETIC MOMENT DYNAMICS

The spin current emitted by a local moment implies angular momentum loss, that is, a dissipative torque acting on the local moment. In the Landau-Lifshitz-Gilbert equation

$$\dot{\mathbf{M}} = -\gamma_{\rm eff}\mathbf{M}\times\mathbf{B} + \frac{\alpha_{\rm eff}}{M_s}\mathbf{M}\times\dot{\mathbf{M}}, \quad (41)$$

spin pumping torques affect the gyromagnetic ratio $\gamma_{\rm eff}$ and enhance the Gilbert damping $\alpha_{\rm eff}$,

$$\gamma_{\rm eff} = \frac{\gamma_0}{1+G_i}, \quad \alpha_{\rm eff} = \frac{\alpha_0 + M_s G_r^{\rm iso}/\gamma_0}{\gamma_0/\gamma_{\rm eff}}, \quad (42)$$

where $\mathbf{M}$ is the magnetization vector, $|\mathbf{M}| = M_s$ is the saturation magnetization, and $\mathbf{B}$ is the sum of external and anisotropy fields acting on the moment. The constants γ_0 and α_0 are the gyromagnetic ratio and Gilbert damping in the absence of spin pumping, respectively. The anisotropic spin pumping currents are not manifest in the magnetization dynamics because their torques vanish when integrated over the local moment. $G_r^{\rm iso}$ and G_i play roles equivalent to the real and imaginary part of the spin mixing conductance at interfaces [1]. $G_r^{\rm iso}$ parameterizes the dissipative angular momentum and energy loss implied by spin pumping, just as the real part of the spin mixing conductance at interfaces.

The imaginary part G_i is sometimes referred to as an "effective magnetic field." It apparently accelerates or decelerates the precessional motion but *conserves energy*. The present results offer a simple picture of the physics of G_i that has escaped attention because it is hidden in the scattering theory formulation of spin pumping: The coherent motion of the proximity RKKY spin density is locked to the precessing magnetization of the local moment. The Zeeman energy of the uncoupled system acts only on the local magnetic moments

$$H_Z^{(0)} = \gamma_0\mathbf{B}\cdot\int\mathbf{S}_{\mathbf{d}}(\mathbf{r},t)d\mathbf{r} = \gamma_0\mathbf{B}\cdot\mathbf{S}(t). \quad (43)$$

On the other hand, it is the entire magnetic moment including the screening spins that precesses

$$\mathbf{M} = -\gamma_0\int[\mathbf{S}_{\mathbf{d}}(\mathbf{r},t) + \mathbf{s}_c(\mathbf{r},t)]d\mathbf{r}, \quad (44)$$

where, in the adiabatic limit,

$$\int\mathbf{s}_c(\mathbf{r},t)d\mathbf{r} = \mathbf{S}(t)\frac{J}{\hbar^2}\int\rho_r(\mathbf{r})d\mathbf{r} = G_i\mathbf{S}(t), \quad (45)$$

so $\mathbf{M}(t) = -\gamma_0(1+G_i)\mathbf{S}(t)$. The Zeeman energy of the coupled systems therefore reads

$$H_Z = \frac{1}{1+G_i}\mathbf{B}\cdot\mathbf{M}(t). \quad (46)$$

The renormalization field $\mathbf{B}\to\mathbf{B}(1+G_i)^{-1}$ is therefore caused by the magnetic screening cloud therefore that can equivalently be written in terms of a new gyromagnetic ratio $\gamma_0\to\gamma_{\rm eff}\equiv\gamma_0(1+G_i)^{-1}$.

V. MAGNETIC INSULATOR/NORMAL METAL INTERFACE

The present results are relevant for an understanding of the anisotropy at interfaces between normal metals and ferromagnetic/ferrimagnetic insulators [29], such as garnets and ferrites. The magnetism is then carried by local atomic moments that are ordered by superexchange interactions, usually via oxygen anions. Since localized on an atomic scale, only moments directly at the interface have a significant exchange interaction with the conduction electrons in the metal. Depending on the crystal direction and the interface cut, the number of

contributing magnetic moments varies, as does the spin mixing conductance [4]. Here we focus on the effects of the crystal field on the spin pumping and the interface spin mixing conductance. The interface can be modelled in terms of independent local moments [4] whose motion is locked by the exchange coupling. The results for the single moments discussed above can then be applied. Cubic sites, such as symmetric octahedrals, do not deform the $3d$ electron density and suppress all anisotropies in cubic ferromagnets. However, at the interface the bulk point symmetry is broken and deformations normal to the interfaces may be expected, although we could not find estimates for the magnitude of such interface crystal fields.

Following Ref. [2], we model the metallic contact as a sheet of magnetic ions in a free electron gas, see Fig. 4(b). Spins can be pumped only in one direction, so we are only interested in the results for $z > 0$, i.e., the metallic side. We introduce the angle β between the interface normal and the local symmetry axes, see Fig. 4(b). For example, when the crystal surface is in (001) and (111) directions, the local symmetry axis is tilted by angles $\beta = 0$ and $\beta \simeq 55^\circ$, respectively. The equilibrium magnetization is assumed to lie in the interface by the thin-film easy-plane form anisotropy that is taken to dominate any perpendicular crystalline magnetic anisotropy. The coordinate along the interface normal z is, in general, not parallel to the coordinate Z that points along the local crystal symmetry axis, see Fig. 4. We adapt Eq. (10) to model the exchange interaction at an interface

$$H_{\rm s-d} = -\frac{J}{\hbar^2}\sum_n \int \mathbf{s}_c(\mathbf{r},t)\cdot\mathbf{S}_d(\mathbf{r}-\mathbf{r}_n,t)d\mathbf{r}, \tag{47}$$

where the moments are at $\mathbf{r}_n = (x_n, y_n, 0)$ in the interface plane and $\mathbf{S}_d(\mathbf{r},t)$ has been defined in Eq. (1). Under FMR conditions all moments precess in phase. We expand the magnetic moment density at the interface into plane waves with reciprocal lattice vectors $\mathbf{G} = G_x\hat{\mathbf{x}} + G_y\hat{\mathbf{y}}$

$$\sum_n n_d(\mathbf{r}-\mathbf{r}_n) = \frac{N_d}{A}\sum_{\mathbf{G}} e^{i\mathbf{G}\cdot(x\hat{\mathbf{x}}+y\hat{\mathbf{y}})} \times \int \frac{dq_z}{2\pi} n_d(q_z\hat{\mathbf{z}}+\mathbf{G})e^{iq_z z}, \tag{48}$$

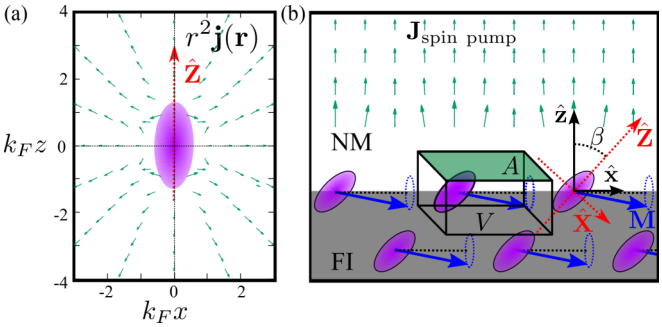

FIG. 4. Anisotropic spin pumping. (a) Dissipative spin current pumped by a single magnetic moment. Far from the origin, the spin current becomes isotropic. (b) Dissipative spin current generated in a bilayer of a ferromagnetic insulator (FI) and normal metal (NM). Far from the interface the spin current direction is normal to the interface. (c) A sheet of magnetic moments is a model for the FI|NM interface.

where N_d is the number of magnetic ions. The proximity conduction electron spin density $\mathbf{s}_c(\mathbf{r},t)$ in linear response is $\mathbf{s}_c(\mathbf{r}) = J\hbar^{-2}[\rho_r(\mathbf{r})\mathbf{S}(t) - \rho_i(\mathbf{r})\dot{\mathbf{S}}(t)]$, where the densities $\rho_{r,i}$ are also periodic in the interface plane,

$$\rho_{r,i}(\mathbf{r}) = \frac{N_d}{A}\sum_{\mathbf{G}} e^{i\mathbf{G}\cdot(x\hat{\mathbf{x}}+y\hat{\mathbf{y}})}\int\frac{dq_z e^{iq_z z}}{2\pi} \times \chi_{r,i}\left(\sqrt{q_z^2+\mathbf{G}^2}\right)n_d(q_z\hat{\mathbf{z}}+\mathbf{G}). \tag{49}$$

The spin conservation equation in the metal reads

$$\nabla\cdot\mathbb{J} = \frac{J^2}{\hbar^4}\mathbf{S}(t)\times\dot{\mathbf{S}}(t)\rho_i(\mathbf{r})\sum_n n_d(\mathbf{r}-\mathbf{r}_n) - \frac{J}{\hbar^2}\dot{\mathbf{S}}(t)\rho_r(\mathbf{r}). \tag{50}$$

In Appendix B we show that the in-plane components of the spin current are exponentially suppressed with distance from the interface with typical decay length of the order of the inverse of the (primitive) reciprocal vector, G^{-1}, which can be estimated as $1\ \text{nm}/(2\pi) = 1.6$ Å, for a lattice constant parameter of 1 nm. The net spin current flow that leaves the magnet is therefore normal to the interface direction as illustrated in Fig. 4(b).

The pumped spin current can be calculated by applying the Gauss theorem to a flat "pill box" with volume $V = Az$ as shown in Fig. 4(b). The spin current in the insulator vanishes, so

$$\int_V \nabla\cdot\mathbb{J}d\mathbf{r} = \mathbf{J}\int_A dxdy, \tag{51}$$

where A is a surface on the metal side at a distance z parallel to the interface and $\mathbf{J}/|\mathbf{J}|$ is the current polarization. Then,

$$\mathbf{J}\int_B dxdy = \frac{J^2}{\hbar^4}\mathbf{S}(t)\times\dot{\mathbf{S}}(t)\int_V d\mathbf{r}\sum_n \rho_i(\mathbf{r})n_d(\mathbf{r}-\mathbf{r}_n) - \frac{J}{\hbar^2}\dot{\mathbf{S}}(t)\int_V d\mathbf{r}\rho_r(\mathbf{r}), \tag{52}$$

which has the solution

$$\mathbf{J} = g_r^{\uparrow\downarrow}\mathbf{m}\times\dot{\mathbf{m}} - g_i^{\uparrow\downarrow}f(z)\dot{\mathbf{m}}, \tag{53}$$

where

$$g_r^{\uparrow\downarrow} = \frac{N_d J^2 S^2}{A\hbar^4}\sum_{\mathbf{G}}\int\frac{d\mathbf{q}}{(2\pi)^3}\chi_i(\sqrt{q^2+\mathbf{G}^2})|n_d(q\hat{\mathbf{z}}+\mathbf{G})|^2, \tag{54}$$

$$g_i^{\uparrow\downarrow} = \frac{N_d S G_i}{A}, \tag{55}$$

and the function $f(z)$ represents the integrated RKKY density in Fig. 6 that can be expressed analytically for short and long distances z from the interface:

$$f\left(z \gg k_F^{-1}\right) \simeq \frac{\cos 2k_F z}{(2k_F z)^2}\left(1 - 2Q_2 k_F^2\frac{3\cos^2\beta - 1}{3}\right), \tag{56}$$

$$f\left(z \ll k_F^{-1}\right) \simeq 1 + 2Q_2 k_F^2\frac{3\cos^2\beta - 1}{9}. \tag{57}$$

The coefficients $g_r^{\uparrow\downarrow}$ and $g_i^{\uparrow\downarrow}$ as obtained by integrating the right-hand side of Eq. (50) represent the real and imaginary

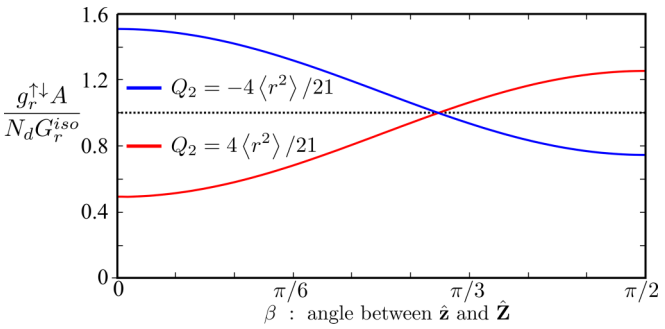

FIG. 5. The dissipative spin current injected by a ferromagnetic insulator into a normal metal $g_r^{\uparrow\downarrow}$ as a function of angle β between crystal field direction and interface normal.

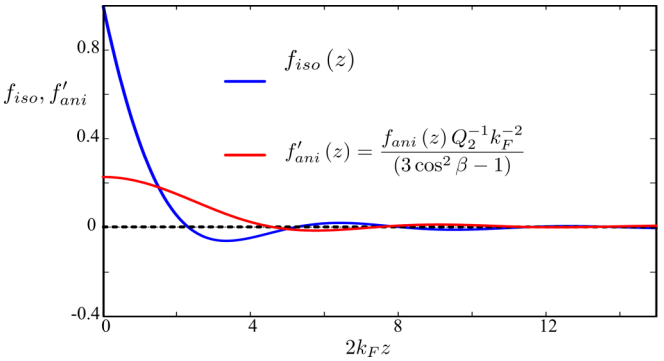

FIG. 6. The RKKY-like spatial oscillation, represented by dimensionless $f(z)$ in the reactive spin current $g_i^{\uparrow\downarrow}f(z)$, where $f = f_{\rm iso} + f_{\rm ani}$ is decomposed into an isotropic ($f_{\rm iso}$) and anisotropic ($f_{\rm ani}$) terms. $f'_{\rm ani}(z) = f_{\rm ani}(z)Q_2^{-1}k_F^{-2}(3\cos^2\beta - 1)^{-1}$ is the normalized $f_{\rm ani}$. For $z \gg k_F^{-1}$, $f_{\rm iso}$ and $f'_{\rm ani}$ approach $(2k_F)^{-2}\cos 2k_F z$ and $-(2/3)(2k_F)^{-2}\cos 2k_F z$, respectively. When $Q_2 \neq 0$ the spin current depends on the angle β.

parts of the spin-mixing conductance, respectively. The sum over $\mathbf{G}$ in Eq. (54) reflects interference effects that can be simplified in the limit of large density of magnetic moments, i.e., when $a \leqslant \pi/k_F$. Since the susceptibility $\chi_i(q)$ is proportional to the step function, see Eq. (19), and modes with wave number $|\mathbf{G}| \geqslant 2k_F$ do not contribute. In that limit

$$g_r^{\uparrow\downarrow} \approx \frac{N_d J^2 S^2}{A\hbar^4}\int \frac{d\mathbf{q}}{(2\pi)^3}\chi_i(q)n_d(q\hat{\mathbf{z}})n_d(-q\hat{\mathbf{z}}) \quad (58)$$

$$= \frac{N_d S^2 G_r^{\rm iso}}{A}\left(1 - Q_2 k_F^2\frac{3\cos^2\beta - 1}{3}\right), \quad (59)$$

where $G_r^{\rm iso}$ is given by Eq. (34). The contribution by Bragg scattering with finite G is relevant for materials with lower interface moment density. However, Eq. (54) as a function of the interface moment density can be calculated only numerically, but we estimate that correction terms suppress the anisotropy. In the dilute limit $N_d \to 0$ all interference and thereby anisotropies vanish, as discussed in Appendix C.

For a $3d^6$ high-spin state of Fe^{2+} or Co^{3+}: $S = 3\hbar/2$ and $N_d/A = (0.5\ \text{nm})^{-2}$, the isotropic contribution $g_r^{\uparrow\downarrow} = N_d S^2 G_r^{\rm iso}/A \sim 10^{18}\ \text{cm}^{-2}$ is of the order of magnitude accepted for magnetic insulators, while $g_i^{\uparrow\downarrow} = N_d S G_i/A \sim 10^{18}\ \text{cm}^{-2}$ appears to be rather large [6]. The anisotropy of the spin current pumped by transition metal ions in an elongated octahedral crystal field and high spin state with $Q_2 = \pm 4/21$ is plotted in Fig. 5. The magnetic ions emit less spin current in the direction in which the $3d$ subshell is elongated, because the spin current is generated by exchange in the overlap volume of the spin densities $\mathbf{s_c}$ and $\mathbf{S_d}$, see Eqs. (30) and (29), and $\mathbf{s_c}$ is preferentially suppressed by proximity in that direction. Ions with positive Q_2 generate maximal (minimal) spin current for $\beta = \pi/2$ ($\beta = 0$), while this is opposite for negative Q_2. The anisotropic spin current depend on the relative angle between the $3d$ subshell orientation and the interface orientation β, which should be observable at selected interfaces.

The reactive spin current depends on position by the function $f(z)$. It is not a transport spin current but is caused by the coherent precession of the proximity spin density. It can be obtained by applying Gauss' theorem to an integral over the volume $V = Az$, as in Fig. 6. The magnitude of this current near the interface is estimated $g_i^{\uparrow\downarrow} \simeq 10^{18}\ \text{cm}^{-2}$ and vanishes algebraically with distance from the interface with the RKKY oscillations. This spatial dependence $f(z)$ is lost in scattering theory in which only the transport of electrons between incoherent reservoirs are considered. The imaginary part of the spin mixing conductance $g_i^{\uparrow\downarrow}$ has been found to be relatively small for most systems [30].

Cobalt ferrite ($CoFe_2O_4$ or CFO) is an iron-based spinel. Cobalt ferrites possess an inverse spinel structure, $[Fe^{3+}]_T[Co^{2+}Fe^{3+}]_O O_4$, where the subscripts $[]_T$ and $[]_O$ stand for the tetrahedral and octahedral sites, respectively. The iron ions have half filled subshell and an isotropic electronic cloud, regardless of the symmetries of their environment. However, the octahedrally coordinated Co^{2+} ions occupy elongated octahedrals when grown on $SrTiO_3$ (STO) substrates. The unit cell lattice parameter of STO $a_{\rm STO} = 3.906$ Å [20] is smaller than the corresponding lattice parameter of CFO $a_{\rm CFO} = 4.195$ Å [20]. As a result of this lattice mismatch, CFO films are in-plane compressed and tetragonally distorted [7,21], depending on the grown direction of the sample. When CFO is grown in the (001) direction, the resultant crystal field is an elongated octahedral, while in the (111) growth direction the compression creates a slanted octahedral crystal field. The resultant crystal field can be described by that of an elongated octahedral with a small energy splitting (see Appendix D). Our model predicts that the exchange between the cobalt ions and the conduction electrons is stronger for a (001) CFO than for a (111) one. Indeed, replacing the cobalt quadrupole $Q_2 = -4/21$ in Eq. (59) for the angles $\beta_{(001)} = 0$ and $\beta_{(111)} = \pi/4$, we find that $g_{r,(001)}^{\uparrow\downarrow}$ is 50% larger than $g_{r,(111)}^{\uparrow\downarrow}$, in agreement with the experiment of Ref. [7]. It should be mentioned that the magnetization and the surface Co^{2+}/Fe^{3+} concentration ratio strongly depend on the preparation conditions [7], however.

Our model can be applied to other than ferromagnetic order of the local moments at the interface. The dissipative spin current emitted by each ion is proportional to $\mathbf{S} \times \dot{\mathbf{S}}$ and thereby invariant to spin reversal $\mathbf{S} \to -\mathbf{S}$. The sum of all spin-current contributions, as well as the real part of the spin mixing conductance, does not depend on the (collinear) order of the sublattices (ferro, ferri, or antiferromagnetic) [4]. However, the imaginary part of the spin mixing conductance

or effective exchange field $g_i^{\uparrow\downarrow}$ felt by the conduction electrons is governed by the sum of the local moments and vanishes for exactly compensated antiferromagnetic interface order. This is consistent with previous studies of the spin pumping by antiferromagnets [31,32].

VI. CONCLUDING REMARKS

The deformations of partially filled $3d$ shells of local moments in noncubic crystal fields are reflected by anisotropic RKKY spin-density oscillations and nonlocal exchange interactions in metallic hosts. We show that the spin current pumped by a magnetic moment with nonspherical spin density is anisotropic as well. The spin pumping leads to enhanced magnetization damping and a renormalized gyromagnetic ratio. The latter can be interpreted in terms of the coherent motion of the RKKY spin density oscillations.

The properties of interfaces between magnetic insulators and metals are governed by the local moments in the terminating monolayer. The spin mixing conductance and its asymmetry depends not only on the density of exposed moments but also on the local point symmetry. We applied the theory to analyze the spin pumping from a ferromagnetic insulator to an adjacent normal metal. Most anisotropies focus the spin currents into a direction normal to the interface, which is beneficial for spintronics. Spin pumping and spin transfer torque are each others Onsager reciprocals and governed by the same spin-mixing conductance. The crystal field effects in spin pumping addressed here therefore equally affect the spin-transfer torque efficiency.

The anisotropy of the pumped spin-current depends on the quadrupole moment Q_2, which in turns depends on the orbital occupation of interface magnetic atoms. While we focus here on CFO, the anisotropy should affect all transition metal based magnetic insulator with magnetic moments at the interface with nonspherical spin distribution. An interesting material to apply the present analysis could be $La_{1-x}Sr_xMnO_3$ (LSMO) in which the $3d$ shell of the Mn ions is not half filled. First principles band structure calculations can test our predictions and render them more quantitative.

ACKNOWLEDGMENTS

A.B.C. acknowledges a JSPS Fellowship for Young Scientists No. JP15J02585. This work was supported by JSPS KAKENHI Grants No. 25247056, No. 25220910, No. 26103006, and CONICYT Becas Chile No. 74170017.

APPENDIX A: TESSERAL SPHERICAL HARMONICS

The $3d$ orbitals can be written as

$$\psi_j(\mathbf{r}) = R_{3d}(r)Y_j(\Omega), \tag{A1}$$

where the radial function can be approximated by Slater-type wave functions [17,18],

$$R_{3d}(r) = \sqrt{\frac{1}{6!}\left(\frac{2}{a}\right)^7} r^2 e^{-r/a}, \tag{A2}$$

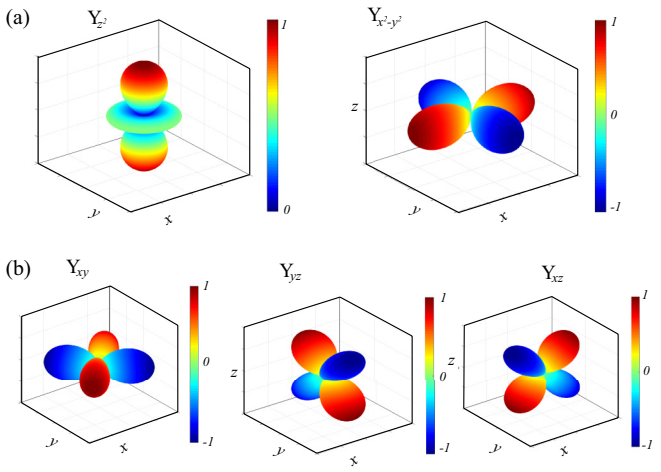

FIG. 7. Orbitals of the $3d$ atomic shell. For each plot, the radius of the surface is the value of the function Y_j, $r(\theta,\phi) = Y_j$, where j is the orbital label. (a) e_g orbitals have lobes along the crystal axes. (b) t_{2g} orbitals point between the axes,.

where the constant a is related to the mean-square radius by $\langle r^2\rangle = 14a^2 \sim 1$ Å. In crystals, the angular part of the $3d$ wave functions is described by the set of orbitals [9]

$$Y_{z^2} = \sqrt{\frac{5}{16\pi}}(3\cos^2\theta - 1) = \sqrt{\frac{5}{16\pi}}\frac{2z^2 - x^2 - y^2}{r^2}, \tag{A3}$$

$$Y_{x^2-y^2} = \sqrt{\frac{15}{16\pi}}\sin^2\theta\cos 2\phi = \sqrt{\frac{15}{16\pi}}\frac{x^2 - y^2}{r^2}, \tag{A4}$$

known as e_g orbitals, and

$$Y_{xy} = \sqrt{\frac{15}{16\pi}}\sin^2\theta\sin 2\phi = \sqrt{\frac{15}{4\pi}}\frac{xy}{r^2}, \tag{A5}$$

$$Y_{yz} = \sqrt{\frac{15}{16\pi}}\sin 2\theta\sin\phi = \sqrt{\frac{15}{4\pi}}\frac{yz}{r^2}, \tag{A6}$$

$$Y_{zx} = \sqrt{\frac{15}{16\pi}}\sin 2\theta\cos\phi = \sqrt{\frac{15}{4\pi}}\frac{zx}{r^2}, \tag{A7}$$

known as t_{2g} orbitals. They are shown in Fig. 7.

1. Mean value of spherical Bessel functions

The nth spherical Bessel function for $n = 0$ and $n = 2$ read

$$j_0(x) = \frac{\sin x}{x}, \tag{A8}$$

$$j_2(x) = \left(\frac{3}{x^2} - \frac{1}{x}\right)\frac{\sin x}{x} - \frac{3\cos x}{x^2}. \tag{A9}$$

Their mean values over Slater-type single-exponential orbitals are

$$\langle j_0(qr)\rangle = \int j_0(qr)n_d(\mathbf{r})d\mathbf{r} = \frac{1 - \frac{5}{6}a^2q^2 + \frac{1}{16}a^4q^4}{\left(1 + \frac{1}{4}a^2q^2\right)^6}$$
$$\approx \left(1 - \frac{q^2\langle r^2\rangle}{6}\right) \tag{A10}$$

$$\langle j_2(qr)\rangle = \int j_2(qr) n_d(\mathbf{r}) d\mathbf{r} = \frac{2a^2q^2(7-3a^2q^2/4)}{15(1+a^2q^2/4)^6} \approx \frac{q^2\langle r^2\rangle}{15}, \quad \text{(A11)}$$

where the approximations are valid for $q^2\langle r^2\rangle \ll 1$.

APPENDIX B: SPIN CURRENT DIRECTION FOR INTERFACES

A two-dimensional periodic lattice is specified by two independent primitive translation vectors, $\mathbf{a}_1$ and $\mathbf{a}_2$

$$\mathbf{r_n} = n_1\mathbf{a}_1 + n_2\mathbf{a}_2. \quad \text{(B1)}$$

Its reciprocal lattice is

$$\mathbf{G} = n_1'\mathbf{b}_1 + n_2'\mathbf{b}_2, \quad \text{(B2)}$$

where $\mathbf{b}_1 = 2\pi\mathbf{a}_2/|\mathbf{a}_1\times\mathbf{a}_2|$ and $\mathbf{b}_2 = 2\pi\mathbf{a}_1/|\mathbf{a}_1\times\mathbf{a}_2|$. Equation (50) implies that translational symmetry of the density n_d and ρ_r carries over to the vector spin potential Φ and spin current tensor $\mathbb{J}^\nu_\sigma(\mathbf{r}) = -\partial_\nu\mathbf{\Phi}(\mathbf{r})$. Therefore

$$\mathbf{\Phi}(\mathbf{r}) = \sum_{\mathbf{G}} \mathbf{\Phi}_{\mathbf{G}}(z) e^{i(G_x x + G_y y)}, \quad \text{(B3)}$$

where the Fourier coefficients $\mathbf{\Phi}_{\mathbf{G}}$ depend on the distance z from the interface. Inserting this expansion into Eq. (50) leads to

$$\left[G^2 - \partial_z^2\right]\mathbf{\Phi}_{\mathbf{G}}(z) = \frac{1}{A}\int_A dxdy e^{-i(G_x x+G_y y)}\boldsymbol{\mathcal{T}}(\mathbf{r}), \quad \text{(B4)}$$

with

$$\boldsymbol{\mathcal{T}}(\mathbf{r}) = -\frac{J}{\hbar}\rho_r(\mathbf{r})\dot{\mathbf{S}} + \frac{J^2}{\hbar^4}\rho_i(\mathbf{r})\sum_n n_d(\mathbf{r}-\mathbf{r}_n)\mathbf{S}\times\dot{\mathbf{S}}, \quad \text{(B5)}$$

where A is the unit cell area. Fourier transforming with respect to z gives

$$\left[G^2 + q_z^2\right]\mathbf{\Phi}_{\mathbf{G}}(q_z) = \boldsymbol{\mathcal{T}}_{\mathbf{G}}(q_z), \quad \text{(B6)}$$

$$\boldsymbol{\mathcal{T}}_{\mathbf{G}}(q_z) = A^{-1}\int dz e^{-iq_z z}\int dxdy e^{-i(G_x x+G_y y)}\boldsymbol{\mathcal{T}}(\mathbf{r}). \quad \text{(B7)}$$

Hence

$$\mathbf{\Phi}(\mathbf{r}) = \sum_{\mathbf{G}} e^{i(G_x x+G_y y)}\int \frac{dq_z e^{iq_z z}}{2\pi\left(q_z^2+G^2\right)}\boldsymbol{\mathcal{T}}_{\mathbf{G}}(q_z) \quad \text{(B8)}$$

$$= \sum_{\mathbf{G}} e^{i(G_x x+G_y y)}\frac{e^{-Gz}}{2G}\boldsymbol{\mathcal{T}}_{\mathbf{G}}(iG), \quad \text{(B9)}$$

using the residuals theorem for the pole $q_z = iG$. $\mathbb{J}$ can be decomposed into the currents along $\mathbf{z}$ and $\mathbf{G}$ as

$$\mathbb{J}^z = \frac{1}{2}\sum_{\mathbf{G}} e^{-Gz}e^{i(G_x x+G_y y)}\hat{\mathbf{z}}\otimes\boldsymbol{\mathcal{T}}_{\mathbf{G}}(iG) \quad \text{(B10)}$$

$$\mathbb{J}^{\mathbf{G}} = \frac{-i}{2}\sum_{\mathbf{G}} e^{-Gz}e^{i(G_x x+G_y y)}\frac{\mathbf{G}}{G}\otimes\boldsymbol{\mathcal{T}}_{\mathbf{G}}(iG), \quad \text{(B11)}$$

where $\otimes$ is the external product of the two subspaces (spin direction and current flow direction). Thus the spin current flowing in the in-plane directions ($\mathbf{J}^{\mathbf{G}}$) decays exponentially with distance z when $\mathbf{G}\neq\mathbf{0}$. Only the contribution perpendicular to the interface ($G=0$) propagates as

$$\mathbf{J}^z(z\gg\langle r\rangle) \sim A^{-1}\int d\mathbf{r}\boldsymbol{\mathcal{T}}(\mathbf{r}), \quad \text{(B12)}$$

which is the same result we obtain in the main text using the divergence theorem. On the other hand, $\mathbf{J}^{\mathbf{G}}$ is not defined for $G=0$.

APPENDIX C: FINITE WAVELENGTH CONTRIBUTIONS TO THE UNIFORM SPIN CURRENT

Corrections for finite $G=|\mathbf{G}|<2k_F$ can be calculated by using the susceptibility $\chi_r(q)$ and spin density $n_d(\mathbf{q})$ in Eqs. (19), (21), and (23) in the spin-mixing conductance formula (54). Equation (54) can be rewritten in terms of lattice vector $\mathbf{a}_{n_x,n_y} = n_x a_x + n_y a_y$,

$$g_r^{\uparrow\downarrow} = \frac{N_d J^2 S^2}{A\hbar^4}\int\frac{d\mathbf{q}}{(2\pi)^3}\chi_i(q)|n_d(\mathbf{q})|^2\sum_{n_x,n_y} e^{i\mathbf{q}\cdot\mathbf{a}_{n_x,n_y}}. \quad \text{(C1)}$$

The numerical integration of the above equation is tedious. However, two natural limit cases are analytically accessible, namely the dense ($a_x,a_y\to 0$) and dilute ($a_x,a_y\to\infty$) local moments approximations. While the former is used in the main text, we address here the second one by the following expansion,

$$e^{i\mathbf{q}\cdot\mathbf{a}_{n_x,n_y}} = 4\pi\sum_{lm} i^l j_l\left(qa_{n_x,n_y}\right)Y_{lm}^*(\hat{\mathbf{q}})Y_{lm}\left(\hat{\mathbf{a}}_{n_x,n_y}\right).$$

For garnets with large lattice constants (large a_n), we can use the asymptotic properties of the spherical Bessel functions,

$$\lim_{qa_{n_x,n_y}\gg 1} j_l\left(qa_{n_x,n_y}\right) = \frac{\sin\left(qa_{n_x,n_y} - l\frac{\pi}{2}\right)}{qa_{n_x,n_y}}. \quad \text{(C2)}$$

Therefore the contribution of the $n_x,n_y\neq 0$ terms decays as $\propto(k_F a_{n_x,n_y})^{-1}$ and for a moment-to-moment distance of a nm and an elemental metal typically smaller than 0.1. The sum of Eq. (C1) is then dominated by the isotropic $n_x=n_y=0$ term and the interface spin-mixing conductance is just the sum of the (isotropic) single ion contributions, $g_r^{\uparrow\downarrow} = NG_r^{\text{iso}}$. The spin current generated by well-separated magnetic moments does cause interference effects on the perpendicular spin current and the anisotropies vanish.

APPENDIX D: CRYSTAL FIELD OF DISTORTED OCTAHEDRAL SITES

Growing CFO films on lattice mismatched substrates [7] causes magnetostriction [33] that leads to a distortion of the octahedral environment of the cobalt moments. An elongation or contraction in the crystal directions (001) and (111) shifts the oxygen ion positions along the direction $(\frac{\sin\beta}{\sqrt{2}},\frac{\sin\beta}{\sqrt{2}},\cos\beta)$, where $\beta_{(001)}=0$ and $\beta_{(111)}=55^\circ$. Similar to Eq. (6), the point charge model leads to a crystal field splitting

$$\Delta H_{cf}^{\beta}(\mathbf{r}) = \Delta_0\frac{2z^2-x^2-y^2}{\langle r^2\rangle}, \quad \text{(D1)}$$

where

$$\Delta_0 = \frac{3\langle r^2\rangle \delta \cos(\beta + \beta_0)}{4\pi\epsilon_0 R_0^3 \cos\beta_0}, \tag{D2}$$

δ is the strain, and $\beta_0 \simeq 35^\circ$. This distortion creates an effective quadrupolar crystal field. The lattice constants of CFO, $SrTiO_3$ substrate, and Pt overlayer are $a_{\mathrm{STO}} = 3.906$ Å, $a_{\mathrm{CFO}} = 4.195$ Å, $a_{\mathrm{Pt}} = 3.912$ Å [34]. With strain $\delta \sim 2\%$, we estimate $\Delta_0 \sim 0.06$ eV.

[1] Y. Tserkovnyak, A. Brataas, and G. E. W. Bauer, Enhanced Gilbert Damping in Thin Ferromagnetic Films, Phys. Rev. Lett. **88**, 117601 (2002).

[2] E. Simanek and B. Heinrich, Gilbert damping in magnetic multilayers, Phys. Rev. B **67**, 144418 (2003).

[3] A. Brataas, Y. Tserkovnyak, G. E. W. Bauer, and P. J. Kelly, in *Spin Current*, edited by S. Maekawa, E. Saitoh, S. Valenzuela, and Y. Kimura (Oxford University Press, New York, 2012), pp. 87–135.

[4] X. Jia, K. Liu, K. Xia, and G. E. W. Bauer, Spin transfer torque on magnetic insulators, Europhys. Lett. **96**, 17005 (2011).

[5] C. Burrowes, B. Heinrich, B. Kardasz, E. A. Montoya, E. Girt, Y. Sun, Y.-Y. Song, and M. Wu, Enhanced spin pumping at yttrium iron garnet/Au interfaces, Appl. Phys. Lett. **100**, 092403 (2012).

[6] M. Weiler, M. Althammer, M. Schreier, J. Lotze, M. Pernpeintner, S. Meyer, H. Huebl, R. Gross, A. Kamra, J. Xiao, Y. Chen, H. Jiao, G. E. W. Bauer, and S. T. B. Goennenwein, Experimental Test of the Spin Mixing Interface Conductivity Concept, Phys. Rev. Lett. **111**, 176601 (2013).

[7] M. Isasa, A. Bedoya-Pinto, S. Velez, F. Golmar, F. Sanchez, L. E. Hueso, J. Fontcuberta, and F. Casanova, Spin Hall magnetoresistance at $Pt/CoFe_2O_4$ interfaces and texture effects, Appl. Phys. Lett. **105**, 142402 (2014).

[8] M. Tokaç, S. A. Bunyaev, G. N. Kakazei, D. S. Schmool, D. Atkinson, and A. T. Hindmarch, Interfacial Structure Dependent Spin Mixing Conductance in Cobalt Thin Films, Phys. Rev. Lett. **115**, 056601 (2015).

[9] S. Blundell, *Magnetism in Condensed Matter* (Oxford University Press, New York, 2001).

[10] S. Maekawa, Y. Tohyama, S. E. Barnes, S. Ishihara, W. Koshibae, and G. Khaliullin, *Physics of Transition Metal Oxides* (Springer, Berlin, 2004).

[11] R. Skomski, *Simple Models of Magnetism* (Oxford University Press, Croydon, 2008).

[12] A. B. Cahaya, A. O. Leon, M. Rahimi, and G. E. W. Bauer (unpublished).

[13] M. A. Ruderman and C. Kittel, Indirect exchange coupling of nuclear magnetic moments by conduction electrons, Phys. Rev. **96**, 99 (1954).

[14] T. Kasuya, A Theory of Metallic Ferro- and Antiferromagnetism on Zener's Model, Prog. Theor. Phys. **16**, 45 (1956).

[15] K. Yosida, Spin Polarization of Conduction Electrons Due to s-d Exchange Interaction, Phys. Rev. **106**, 893 (1957).

[16] L. Zhou, J. Wiebe, S. Lounis, E. Vedmedenko, F. Meier, S. Blügl, P. H. Dederichs, and R. Wiesendanger, Strength and directionality of surface Ruderman-Kittel-Kasuya-Yosida interaction mapped on the atomic scale, Nat. Phys. **6**, 187 (2010).

[17] A. J. Freeman and R. E. Watson, Theoretical investigation of some magnetic and spectroscopic properties of rare-earth ions, Phys. Rev. **127**, 2058 (1962).

[18] J. T. Waber and D. T. Cromer, Orbital Radii of Atoms and Ions, J. Chem. Phys. **42**, 4116 (1965).

[19] C. Housecroft and A. G. Sharpe, *Inorganic Chemistry*, 3rd Ed., (Prentice Hall, London, 2008).

[20] M. Valant, A.-K. Axelsson, F. Aguesse, and N. M. Alford, Molecular auxetic behavior of epitaxial co-ferrite spinel thin film, Adv. Funct. Mater. **20**, 644 (2010).

[21] M. N. Iliev, D. Mazumdar, J. X. Ma, A. Gupta, F. Rigato, and J. Fontcuberta, Monitoring B-site ordering and strain relaxation in $NiFe_2O_4$ epitaxial films by polarized Raman spectroscopy, Phys. Rev. B **83**, 014108 (2011).

[22] U. Larsen, A simple derivation of the sd exchange interaction, J. Phys. C **4**, 1835 (1971).

[23] D. Davis, Thomas-Fermi screening in one dimension, Phys. Rev. B **7**, 129 (1973).

[24] H. Adachi, K. Uchida, E. Saitoh, and S. Maekawa, Theory of the spin Seebeck effect, Rep. Prog. Phys. **76**, 036501 (2013).

[25] A. B. Cahaya, O. A. Tretiakov, and G. E. W. Bauer, Spin Seebeck power conversion, IEEE Trans. Magn. **51**, 0800414 (2015).

[26] B. Mihaila, arXiv:1111.5337.

[27] Y.-T. Chen, S. Takahashi, H. Nakayama, M. Althammer, S. T. B. Goennenwein, E. Saitoh, and G. E. W. Bauer, Theory of spin Hall magnetoresistance, Phys. Rev. B **87**, 144411 (2013).

[28] B. Dieny and M. Chshiev, Perpendicular magnetic anisotropy at transition metal/oxide interfaces and applications, Rev. Mod. Phys. **89**, 025008 (2017).

[29] In metallic systems the 3*d* orbitals strongly hybridize with 4*s* bands and the local moment picture advocated here is less applicable.

[30] M. Zwierzycki, Y. Tserkovnyak, P. J. Kelly, A. Brataas, and G. E. W. Bauer, First-principles study of magnetization relaxation enhancement and spin transfer in thin magnetic films, Phys. Rev. B **71**, 064420 (2005).

[31] R. Cheng, J. Xiao, and Q. Niu, and A. Brataas, Spin Pumping and Spin-Transfer Torques in Antiferromagnets, Phys. Rev. Lett. **113**, 057601 (2014).

[32] S. Takei, B. I. Halperin, and A. Yacoby, and Y. Tserkovnyak, Superfluid spin transport through antiferromagnetic insulators, Phys. Rev. B **90**, 094408 (2014).

[33] F. Rigato, J. Geshev, and V. Skumryev, and J. Fontcuberta, The magnetization of epitaxial nanometric $CoFe_2O_4$ (001) layers, J. Appl. Phys. **106**, 113924 (2009).

[34] T. Dhakal, D. Mukherjee, R. Hyde, P. Mukherjee, M. H. Phan, H. Srikanth, and S. Witanachchi, Magnetic anisotropy and field switching in cobalt ferrite thin films deposited by pulsed laser ablation, J. Appl. Phys. **107**, 053914 (2010).